PHOTOMASK

BACUS—The international technical group of SPIE dedicated to the advancement of photomask technology.

SPIE Photomask Technology + EUV Lithography
1st Place Winner - Zeiss Award

EMA Modelled Alternative EUV Absorber Materials Considering Optical and Stability Behavior

Rajiv N. Sejpal and Bruce W. Smith, Microsystems Engineering, Kate Gleason College of Engineering, Rochester Institute of Technology, Rochester, NY 14623

ABSTRACT

Alternatives to Ta-based absorbers are being considered for next generation lithography nodes to reduce 3D mask effects and to improve image modulation through phase interference. Low complex refractive index ($n - ik$) materials can provide phase shifting behavior at thicknesses less than those needed for conventional absorbers, essentially acting as attenuated phase shift mask (attPSM) films. Identifying attPSM absorber thickness and consequent phase requires determining optimum phase shift mask reflectance. Imaging with absorbers at high reflectance show better imaging performance. The absorber thickness is determined where the interference effects lead to high absorber reflectivity. Low refractive index (n) materials are therefore desired as candidate attPSM absorbers. Low – n material combinations identified using Wiener bounds and Effective media approximation (EMA) modelling are optimized for NILS and MEEF using absorber reflectivity on-line-space and contact-holes patterns. Absorber candidates at optimum thickness for contact holes are compared with conventional Ta-based absorber using reflected nearfield intensity imaging.

1. Introduction

EUV lithography at 0.33 numerical aperture (NA) as implemented uses a 55 – 70nm Ta-based mask absorber. The current EUV mask illuminated at oblique illumination angles introduces mask induced imaging effects that lead to contrast loss. Imaging the next technological nodes with current mask architecture will be extremely challenging. Fig. 1(a) shows the loss of aerial image NILS with pitch scaling for line-space and contact holes patterned using a Ta-based absorber. Therefore, the semiconductor manufacturing industry has shifted its focus on finding a thinner, alternative mask absorber candidate. Two alternative optical designs proposed are the masks with high extinction coefficient (high – k) and low refractive index (low – n) attenuated phase shifting mask (attPSM) absorbers. Thinner mask absorber candidates possess the capability to alleviate some 3D mask effects in addition to improved aerial image normalized image log slope (NILS), lower dose to size and higher depth of focus.[1,2]

High NILS is desired to achieve lower line width roughness (LWR), better CD uniformity (LCDU) and hence, lower stochastic effects.[3] Higher NILS associated with the phase shifting masks have also shown to improve image fidelity compared to the conventional Ta – based masks. Identifying absorber candidate materials that maximize NILS is therefore a priority. Additionally, shrinking feature sizes in the future nodes will experience enhanced mask effects as shown in Fig. 1(b). Therefore, co-optimizing mask error enhancement

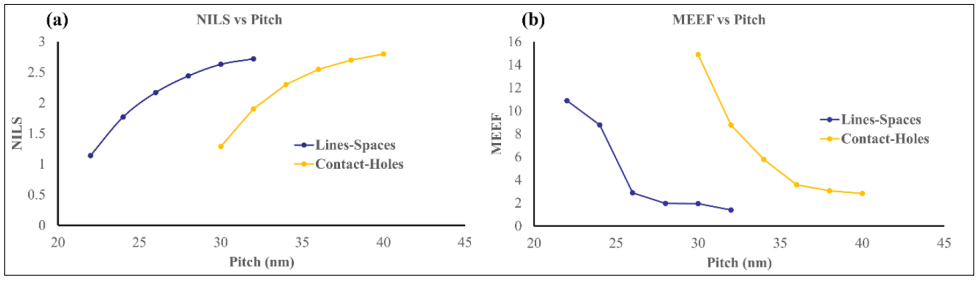

Figure 1. (a) NILS vs Pitch for dense lines-spaces and contact hole patterns and (b) MEEF vs Pitch for dense lines-spaces and contact-hole patterns for a conventional Ta-absorber mask stack.

BACUS NEWS

JANUARY 2022
VOLUME 38, ISSUE 1

Nick Cobb Scholarship winner

Yonghwi Kwon has been announced as the 2022 recipient of the $10,000 Nick Cobb Memorial Scholarship by SPIE, the international society for optics and photonics, and Siemens EDA – formally Mentor, a Siemens company – for his potential contributions to the field related to advanced lithography. https://spie.org/x139160.xml

TAKE A LOOK INSIDE:

SPIE.

11855-7

EDITORIAL

Deep Learning Needs Lots of Data and Data of Your Choice: Digital Twins are the Solution

Aki Fujimura, D2S, Inc.

Deep learning (DL) has become an integral part of the success of many companies – and not just the Amazons and Googles of the world, but also manufacturing companies like GE and Tesla. So why doesn't it play a larger role for semiconductor manufacturing yet? There have been many papers and some reported successes, yet only 22% of the luminaries participating in the 2021 eBeam Initiative Luminaries survey see DL becoming a competitive advantage by next year. Why?

DL prototypes are relatively easy to create, but applying that prototype to production is much, much harder. The gap between prototype and production is data. A lot of data. DL is "programmed" and tuned through the data presented to the neural networks. If the goal of the application is to, for instance, identify fatal mask errors, the neural nets must be presented with millions of examples of the fatal errors to train the network to recognize them.

And this is a big problem for our industry, for two reasons. First, the data used by mask makers does not belong to them – it belongs to their customer, or even their customer's customer. Vendors developing DL applications for mask makers cannot get enough data to sufficiently train a DL for production deployment. Second, DL networks for many applications need to be trained with a sufficient volume of anomalous data to be able to identify a wide range of error conditions. But mask makers take great pains to avoid such anomalies and so such data is in short supply. Anomalous data could be created using standard mask making techniques, but this uses scarce and expensive production resources and doesn't produce data in sufficient volume for DL training.

So, how do we solve the data problem for our industry? Digital twins are the answer. Digital twins – digital representations of real-world equipment and processes – can produce the volume of data required for successful DL. Most crucially, they can produce whatever kind of data is required, in the volumes required. The process of moving from DL prototype to DL production application means tuning the DL networks with very specific data to meet the specific task at hand.

Take the ubiquitous example of a DL network that can identify cats from dogs, and within those categories, identify specific breeds of each animal. If this DL network misclassifies an American Shorthair cat as an Egyptian cat, you need to get the data to train the network to correctly identify American Shorthair cats. In this case, that data is easily available on the internet. However, for semiconductor manufacturing, there is no "ImageNet" of SEM images to use to clarify classifications for a DL network. Physically creating this data is far too expensive and time-consuming – especially because the process of refining a DL network for production-level accuracy involves many, many rounds of training/inferencing/tuning.

This is why digital twins – whether in the form of simulation or DL-based digital twins – play such a critical role in developing production-worthy DL applications. Many papers have been presented that provide good roadmaps for creating and using digital twins in semiconductor manufacturing, most notably by the participants in the Center for Deep Learning for Electronics Manufacturing, or CDLe (cdle.ai).

There is no reason that DL can't be as important a factor for success for semiconductor manufacturing as it is in so many other industries. The road ahead is clear: careful application, commitment of resources over time, and most importantly, using digital twins to create the massive volumes of data required for DL production success.

BACUS

N • E • W • S

BACUS News is published monthly by SPIE for *BACUS*, the international technical group of SPIE dedicated to the advancement of photomask technology.

Managing Editor/Graphics Linda DeLano
SPIE Sales Representative, Exhibitions, and Sponsorships Melissa Valum
BACUS Technical Group Manager Tim Lamkins

■ **2022 BACUS Steering Committee** ■

President
Emily E. Gallagher, *imec.*

Vice-President
Kent Nakagawa, *Toppan Photomasks, Inc.*

Secretary
Jed Rankin, *GLOBALFOUNDERIES Inc.*

Newsletter Editor
Artur Balasinski, *Infineon Technologies*

2022 Photomask + Technology Conference Chairs
Bryan S. Kasprowicz, *HOYA*
Ted Liang, *Intel Corp.*

Members at Large
Frank E. Abboud, *Intel Corp.*
Uwe F. W. Behringer, *UBC Microelectronics*
Ingo Bork, *Siemens EDA*
Tom Cecil, *Synopsys, Inc.*
Aki Fujimura, *D2S, Inc.*
Jon Haines, *Micron Technology Inc.*
Naoya Hayashi, *Dai Nippon Printing Co., Ltd.*
Henry Kamberian, *Photronics, Inc.*
Bryan S. Kasprowicz, *HOYA*
Romain J Lallement, *IBM Research*
Jan Hendrik Peters, *bmbg consult*
Douglas J. Resnick, *Canon Nanotechnologies, Inc.*
Thomas Scheruebl, *Carl Zeiss SMT GmbH*
Ray Shi, *KLA Corp.*
Thomas Struck, *Infineon Technologies AG*
Anthony Vacca, *Automated Visual Inspection*
Vidya Vaenkatesan, *ASML Netherlands BV*
Andy Wall, *HOYA*
Michael Watt, *Shin-Etsu MicroSi Inc.*
Larry Zurbrick, *Keysight Technologies, Inc.*

SPIE.

P.O. Box 10, Bellingham, WA 98227-0010 USA
Tel: +1 360 676 3290
Fax: +1 360 647 1445
SPIE.org
help@spie.org

©2022

All rights reserved.

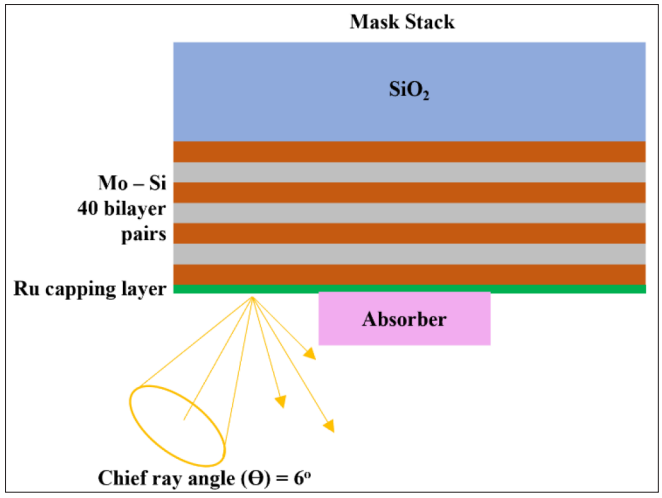

Figure 2. EUV mask stack with 40 Mo/Si bilayer pairs on a SiO_2 substrate followed by a Ru capping layer and the absorber.

the mask absorber thickness is varied within the range of 25 – 55nm to simulate the effect of the varying reflectance.

2.1 Lines - Spaces

Equal line/space patterns are illuminated with a dipole source. The sigma center (σ_c) and sigma radius (σ_r) are determined using Eqs. (1) and (2). Here, λ is the source wavelength, p is the pitch and, NA_o and NA_c are the numerical aperture of the objective and condenser lenses, respectively. For a 30nm pitch, σ_c = 0.68 and σ_r = 0.31.

$$\sigma_c = \frac{\lambda}{2pNA_o} \quad (1)$$

$$\sigma_r = \frac{NA_c}{NA_o} \quad (2)$$

Figure 3(a) shows the aerial image NILS and reflectivity versus the absorber thickness for an attPSM candidate absorber. The reflectivity values are normalized to multilayer mirror (with capping layer) reflectivity at CRA = 6°. The interference effects of a phase shifitng mask are projected on the image plane that causes NILS swing. The reflectivity trend gradually increases with reduction in the absorber thickness. NILS

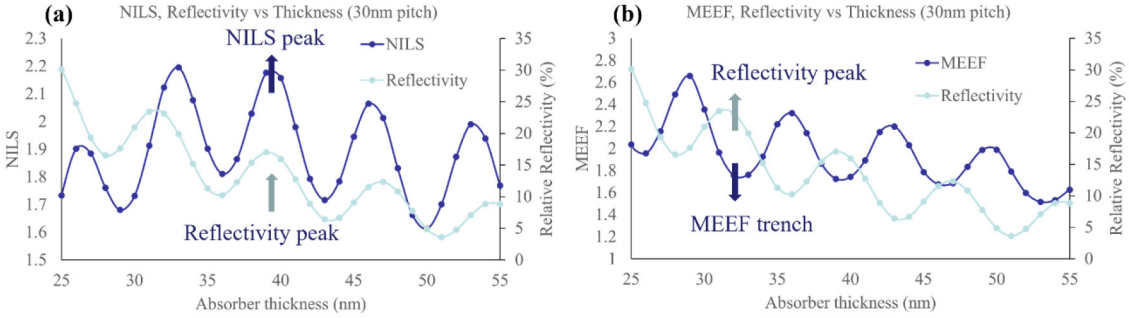

Figure 3. (a) NILS, reflectivity vs absorber thickness for a 30nm pitch line/space pattern. (b) MEEF, reflectivity vs absorber thickness for line/space pattern.

factor (MEEF) with NILS is necessary. The overall imaging performance of the phase shifting mask depends on the optical characteristics of the absorber. Mask absorbers with relatively of low refractive index ($n - ik$) values at 13.5nm wavelength can exhibit high reflectance, phase shifting behavior. Materials and combinations within this region of refractive index spectrum can serve as attenuated phase shifting mask absorbers. The reflectivity and phase requirements of the candidate materials depend on the layout and design requirements. The choice of absorber reflectivity will determine the absorber thickness and the phase.

Designing a robust attenuated phase shifting mask is a two-fold challenge. Determining the suitable optical properties for best imaging metrics and, identifying candidate absorber materials that meet the mask design requirements. We present an approach to identify the optimum absorber reflectivity through co-optimization of NILS and MEEF on EMA modelled phase shifting absorber candidates for line-space and dense contact-hole patterns.

2. Ideal Mask Reflectivity

To determine the ideal reflectance, a 3D mask is designed using the Prolith Simulator.[4] The mask stack includes a multilayer mirror of 40 Mo (3nm)/Si (4nm) bilayer pairs on a 20nm SiO_2 substrate followed by a 2nm ruthenium capping layer and the absorber, as shown in Fig. 2. The mask stack is illuminated with a 13.5nm source wavelength at a chief ray angle (CRA) of 6°. A line/space pattern at a pitch of 30nm and contact-holes pattern at pitch of 40nm are used test cases to determine the ideal mask absorber reflectivity and thickness for best NILS and MEEF. While the multilayer mirror will also influence the overall mask reflectivity, only

trend also improves as the height of the absorber is reduced to 30nm, beyond which the NILS degrades. NILS value peaks with peak in the absorber reflectivity as indicated by the arrows. Fig. 3(b) plots the MEEF and reflectivity against the absorber thickness. Similar to NILS, MEEF trend gradually increases with absorber reflectivity. However, MEEF obseves a trench when the reflectivity peaks. Suitable values of NILS and MEEF are observed at reflectivity peaks. Highly reflectance attPSM absorbers are therefore desired. Furthermore, within the desired 30 – 45 nm absorber thickness range, the reflectivity peaks 2 to 3 times. This corresponds to multiple optimum thickness ranges. Appropriate mask absorber thickness can then be chosen based on design and processing requirements. For example, a 40nm absorber thickness will have an aerial image NILS of 2.15 at 16% mask reflectivity and phase shift of approximately 233°.

2.2 Contact - Holes

Similar to line/space patterns, contact-holes are also co-optimized to determine the impact of mask reflectivity on imaging performance. Dense contact-holes array with a 40nm pitch (x- and y-pitch) is illuminated with a quadrupole light source. The σ_c = 0.72 and σ_r = 0.31 values are determined using Eqs. (3) and (2), respectively.

$$\sigma_c = \frac{\lambda}{\sqrt{2}pNA_o} \quad (3)$$

Figure 4(a) & (b) show the NILS and MEEF vs. absorber thickness and reflectivity, respectively. NILS behavior of contact-holes is similar to that of line/space pattern. NILS peaks with peak in the absorber reflectivity.

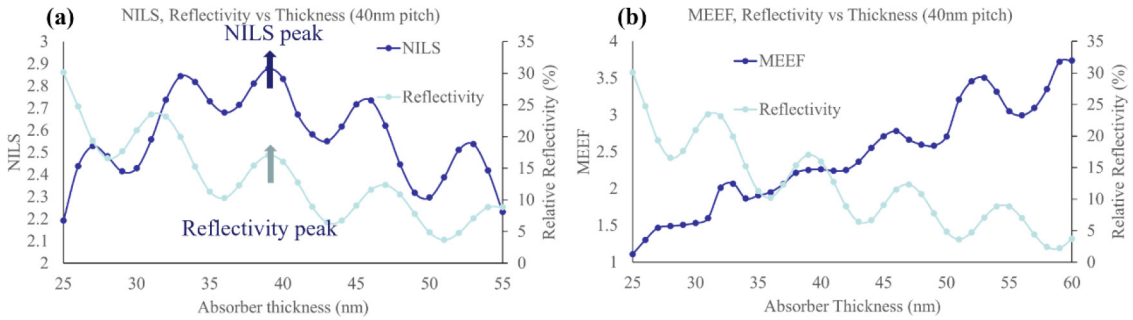

Figure 4. (a) NILS, reflectivity vs absorber thickness for 40nm pitch contact-holes array. (b) MEEF, reflectivity vs absorber thickness for 40nm pitch contact-holes array.

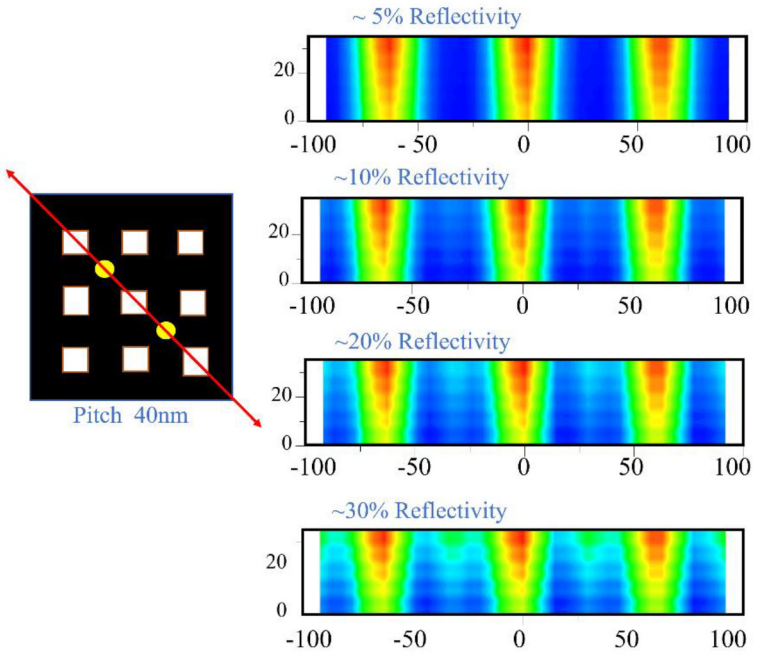

Figure 5. Contact-holes imaged on a 35nm generic EUV resist using Prolith Simulator. The measurements are observed diagonally as indicated by the red arrow. False contacts appear between the corners of the contacts as depicted by yellow circles.

However, unlike lines and spaces, the overall trend of MEEF reduces with absorber thickness. Furthermore, MEEF swing is less pronounced and the trench in MEEF swing does not occur with reflectivity peak. MEEF is therefore more dominant and, an appropriate value of absorber reflectivity and thickness can be chosen when MEEF is below acceptable tolerances.

Although high absorber reflectance is desired for optimum NILS and MEEF, care must be exercised in determining the appropriate reflectivity values to avoid printing false contacts that may lead to stochastic failures. Figure 5 demonstrates this effect by plotting the image in the resist as the absorber reflectivity increased from 5% and 30%. False contacts at diagonal locations begin to appear in the resist for relative reflectivity values of 20% and above, indicated by yellow spots.

As the absorber reflectivity increases, intensity of false contact (FC) increases and, the relative aerial image (AI) intensity associated with the clear areas of the contact-holes decreases. This can be characterized using the false contact ratio (FCR) in Eq. (4). Figure 6 plots the FCR vs absorber thickness and reflectivity. The FC ratio should be as large as possible to reduce the probability of stochastic failures. Therefore, a trade-off exists between the imaging performance and FCR ratio.

$$FCR = \frac{AI\ Intensity}{FC\ Intensity} \tag{4}$$

3. Materials Modelling Using EMA

Identifying materials and combinations that satisfy the optical design requirements for attenuated phase shifting mask absorber is challenging. As we are interested in materials that act as high reflection phase shifting mask absorbers, we need materials with low refractive index values (low n – low k). Standard thin films considerations, such as in Eqs. (5) & (6) in combination with k – n plots at 13.5nm enable recognizing the regions of the refractive index spectrum that meet the design requirement. As few single elements meet the high reflectivity and phase characteristics essential for optimum imaging performance, candidate absorbers are most likely alloys and/or compounds.

$$\Delta\emptyset = \frac{4\pi d}{\lambda cos\theta}(1-n) \tag{5}$$

$$k = \frac{\ln\left(\frac{1-R}{T}\right)}{2\Delta\emptyset}(n-1) \tag{6}$$

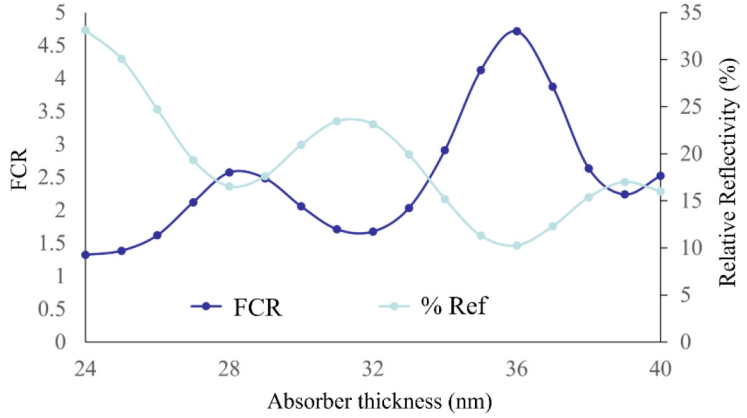

Figure 6. False contact intensity characterization using FCR ratio. Larger FCR ratio is desired to reduce the probability of stochastic failures.

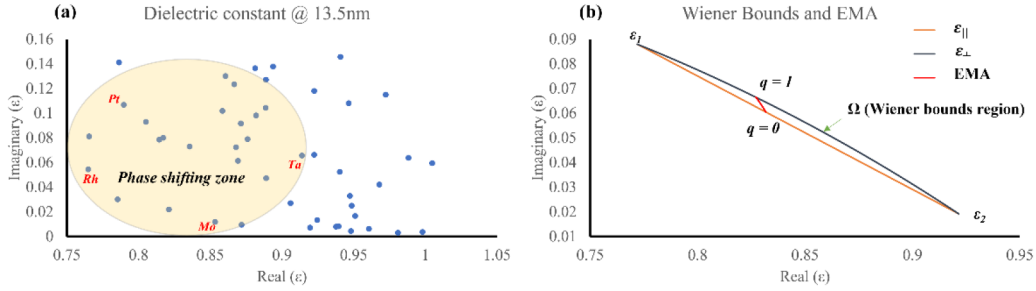

Figure 7. (a) Variety of materials plotted in the complex dielectric constant spectrum. Materials in the highlighted region can exhibit phase shifting behavior. The elements in Pt, Rh, Mo and Pt are used in this study. (b) Wiener Bounds and EMA model for arbitrary ε_1 and ε_2 values. The EMA model is calculated for fraction volumes $f_1 = 0.6$ and $f_2 = 1 - f_1 = 0.4$.

Here, $\Delta\varnothing$ is the phase shift, d is the thickness, n is the refractive index, k is the extinction coefficient, T is transmission function or the absorber reflectivity and, R is the reflection function.

$$\varepsilon = (n + ik)^2 \tag{7}$$

It is convenient to discuss and model alloys using the complex dielectric constant in Eq. (7) rather the refractive index. Figure 7(a) plots a of variety of materials in the dielectric constant space. For this purpose, we employ dielectric constant modelling using Wiener Bounds[5] and Effective Media Approximation model.[6,7] Wiener Bounds are the extreme bounds on the value of the effective dielectric constant ε_{eff} of a composite material. Wiener Bounds are defined by determining the dielectric response of the composite to the incident light with its electric field vector perpendicular ($\varepsilon_{\perp}$) and parallel to the structure ($\varepsilon_{||}$). The underlying assumption is that the individual layers or nanoparticles, such as employed in a multilayer system, are smaller than the 13.5nm source wavelength. The region (Ω), as shown in Fig. 7 (b), defined by the Wiener Bounds of the effective media is dependent on the complex dielectric constants (ε) of the individual constituents and the material stoichiometry. ε_1 and ε_2 are the complex dielectric constant of the constituent elements.

By using effective medium models in conjunction with Wiener Bounds, a specific value of the effective dielectric constant (ε_{eff}) can be determined. We employ Effective Media Approximation (EMA) model that employs a material depolarization factor (q). The ε_{eff} using the EMA model can be calculated using Eq. (8). The EMA model incorporates the effects of the surrounding medium (or the host medium) on the elemental loading medium through the screening parameter $\bar{\varepsilon}$, shown in Eq. (9). The q factor depends on the geometrical shape and orientation of the suspended nanoparticles in the composite. The value of q ranges from 0 to 1 and in case of spherical nanoparticles with perfect mixing, the q factor assumes a value of 1/3. An example of EMA model for a two-material system is shown by the red line in Fig. 7(b). The EMA model is calculated for volumetric fractions $f_1 = 0.6$ and $f_2 = 0.4$ corresponding to materials with dielectric constants ε_1 and ε_2, respectively.

$$\varepsilon_{eff} = \frac{\varepsilon_1\varepsilon_2 + \bar{\varepsilon}(f_1\varepsilon_1 + f_2\varepsilon_2)}{\bar{\varepsilon} + (f_1\varepsilon_2 + f_2\varepsilon_1)} \tag{8}$$

where,

$$\bar{\varepsilon} = \frac{(1-q)\varepsilon_{host}}{q} \tag{9}$$

Four alloys from three binary refractory metal systems, specifically Rh – Ti, Mo – Pt and, Rh – Ta, are identified as candidate absorber materials capable of generating relatively high mask reflectivity. The chosen elements in the dielectric constant spectrum are shown in Fig. 7(a). The Wiener bounds of the refractory metal systems along the EMA models of alloys are shown in Fig. 8. The fractional volumes are calculated using the fractional weights obtained from thermodynamic phase diagrams and theoretical material densities.[8] The effective dielectric constants for all the alloys are calculated for a depolarization factor (q) = 1/3. The effective dielectric constants are translated back to the refractive index domain and tabulated in table 1 below.

4. Imaging Performance Characterization

4.1 Lines – Spaces

All four candidate alloys identified can generate relatively high reflectance at reduced thickness when employed as attPSM absorbers. The litho-

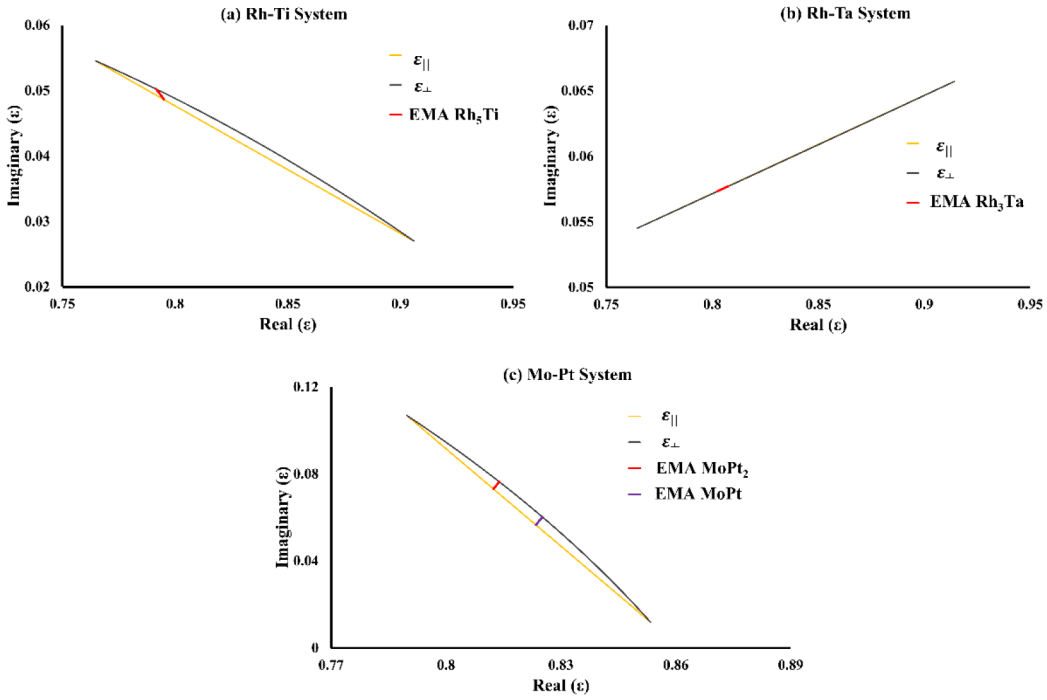

Figure 8. (a) Wiener Bounds for Rh – Ti system and EMA model for Rh_5Ti alloy. (b) Wiener Bounds for Rh – Ta system and EMA model for Rh_3Ta alloy. (c) Wiener Bounds for Mo – Pt system and EMA models for MoPt and MoPt alloys.

Table 1. Complex effective dielectric constants and refractive indices for EMA modelled alloys.

Material Composition	Dielectric constant		Refractive index	
	ε_r	ε_k	n	k
Rh_5Ti	0.7938	0.0492	0.8914	0.0276
Rh_3Ta	0.8057	0.0575	0.8982	0.0320
$MoPt_2$	0.8128	0.0741	0.9025	0.0410
MoPt	0.8240	0.0577	0.9083	0.0317

graphic performance of each mask absorber candidate is evaluated for line/space patterns through pitch. The absorber thickness is co-optimized for best NILS and MEEF within the range of 25 – 55nm. Dipole is used as the illumination source with optimized σ_c and σ_r values using Eqs. (1) and (2). Figure 9(a) – (d) show the NILS performance of the identified absorber candidates versus absorber thickness and reflectivity. Rh_5Ti produces highest absorber reflectivity because of its low extinction coefficient. NILS for each absorber is characterized for 24nm, 26nm, and 30nm pitches, respectively. Scaling pitch degrades the aerial image NILS substantially for all the absorber candidates. Two high NILS peaks corresponding to the respective reflectivity peaks for each absorber candidate are highlighted in the desired thickness range. This results in two high NILS absorber thickness values.

The choice of a singular optimum thickness depends on the co-optimization of NILS and MEEF along with the desired phase shift. Rh_5Ti generates greater NILS at 20% reflectivity corresponding to 33nm absorber thickness. However, MEEF value at 33nm is also higher than at 39nm absorber thickness. Hence, the optimum thickness for Rh_5Ti will depend on the MEEF tolerance for a given design/process. Additionally, the phase shift of Rh_5Ti at 33nm is approximately 192°. This value is much lower than the desired 1.2π phase equired to correct the M3D effects associated with the EUV lithography.[9,10] Figure 10 plots the MEEF response for all absorbers at respective pitches. MEEF degrades at smaller pitches however, all candidate absorbers have a comparable MEEF response. Individual NILS for each absorber at optimized thickness are listed in Table 2 along with the relative reflectivity and phase shift values.

Based on NILS and MEEF co-optimization, the ideal absorber thickness for line/space pattern is 39nm for Rh_5Ti, Rh_3Ta and $MoPt_2$. Optimum absorber thickness for MoPt alloy is 46nm. The higher thickness at optimum phase shift for MoPt alloy is due to the relatively higher *n* value compared to other absorber candidates. This suggests low *n* – low *k* refractive index combination is most desired for a thin, high fidelity imaging in EUV.

4.2 Contact – Holes

Identified absorber candidates are also evaluated on contact-holes using NILS and MEEF co-optimization to determine best absorber thickness. Figure 11 plots the aerial image NILS response of dense contact-holes array at 36nm and 40nm pitch using the attPSM absorber candidates, respectively. Highlighted regions show higher NILS values in the desired

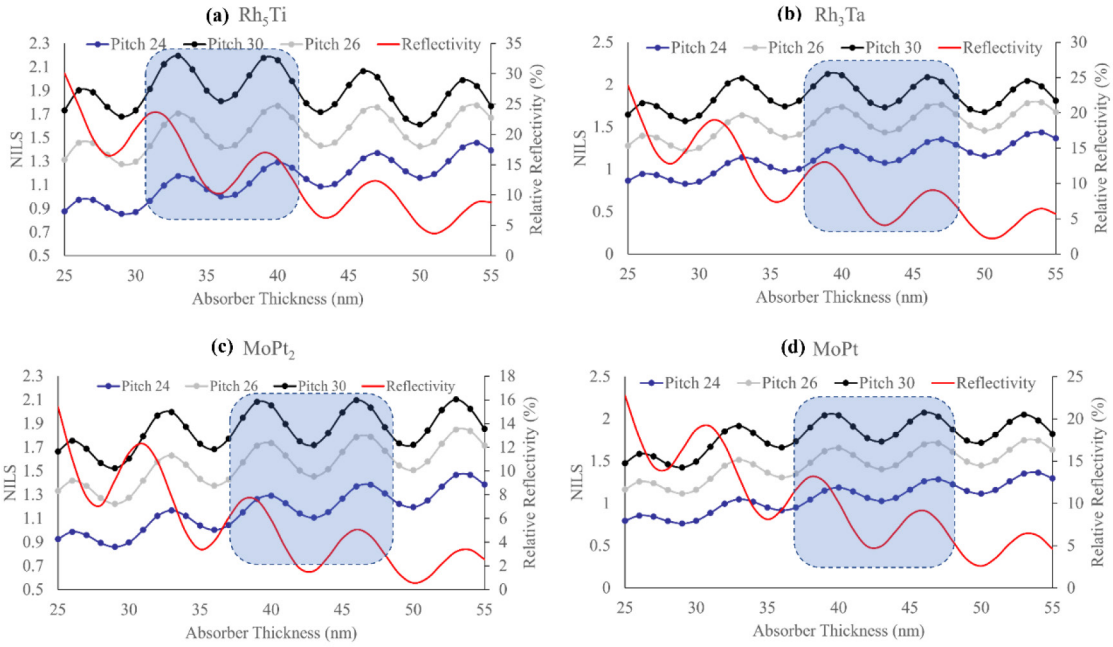

Figure 9. NILS, reflectivity vs absorber thickness of 24nm, 26nm, and 30nm line/space pitch imaged using (a) Rh_5Ti mask absorber stack, (b) Rh_3Ta mask absorber stack, (c) $MoPt_2$ mask absorber stack and (d) MoPt mask absorber stack.

Table 2. Aerial image NILS for 24nm, 26nm, and 30nm line/space pitch imaged at optimized thickness for candidate absorbers along with associated reflectivity and phase shift values.

Absorber	NILS			Reflectivity (%)	Phase Shift (°)
	24nm	26nm	30nm		
Rh_5Ti @ 39m	1.23	1.71	2.17	17%	227°
Rh_3Ta @ 39m	1.22	1.69	2.12	13%	213°
$MoPt_2$ @ 39m	1.26	1.71	2.08	7.5%	204°
MoPt @ 46m	1.26	1.7	2.07	9.14%	226°

thickness range of the mask absorber. Although the NILS in the highlighted regions peaks at 39nm absorber thickness, the MEEF dictates the thickness to be at 42nm, as seen in Fig. 12 below. Table 3 lists the NILS at individual pitches for absorber candidate at 42nm thickness.

Choice of a lower absorber thickness around 35nm in case of contact-holes can be argued due to lower MEEF values for a small compromise in NILS. However, the phase shifts associated with the reduced thickness are much lower from the desired 1.2π. This may negatively influence the M3D effects. Controlling MEEF below tolerance values will enable higher NILS at higher mask reflectance. Although, lower relatively lower attPSM reflectance in case of contact-holes may be advantageous to reduce the probability of stochastic failures, as lower reflectance leads to lower FCR ratio.

We also investigate the reflected nearfield intensity of contact-holes at 40nm pitch with a 20nm opening. Reflected nearfield intensity plots help visualize absorber performance under EUVL illumination conditions. Figure 13 plots the reflected nearfield intensities for candidate attPSM absorbers at optimized 42nm thickness along with a 61nm Ta-based absorber. The intensities are plotted for CRA = 6° and 10°. Intensity imbalance at larger illumination angles indicate significant impact of illumination conditions at the mask plane. This may increase M3D effects and negatively impact image contrast.[11] The effects of oblique illumination angle can be clearly observed for Ta – based reference absorber. The intensity loss is even greater when CRA is 10°. In comparison, attPSM candidate absorbers experience reduced intensity loss at both incidence angles.

5. Conclusion

Extensive research on attenuated phase shifting mask absorbers for EUV lithography has shown to improve image contrast, dose to size and even extenuate some M3D effects. However, the main challenge is to determine and characterize the best optical design and then, identify materials that satisfy these design requirements. We have presented an approach to investigate the desired optical properties of absorbers using attPSM reflectance. EMA modelled refractory metal alloys as absorber candidates that satisfy the reflectivity requirements are also presented.

AttPSM absorbers candidates are found to perform better at high reflectivity values. In case of line-space pattern, NILS swing due to interference effects peaks when absorber reflectivity peaks. Co-optimization with MEEF show a minima in MEEF swing at reflectivity peaks. However, MEEF trend gradually increases with increase in the absorber reflectivity. An optimum thickness of 39nm is identified for all candidate absorbers using the NILS and MEEF cooptimization except the MoPt alloy. MoPt used as an attPSM mask absorber has an optimized thickness range of 46nm. The phase shift values at optimized thickness for all candidate alloys are closer to the 1.2π phase shift required to correct for M3D effects. The higher thickness of the MoPt absorber is due to a relatively higher *n* value. Therefore, low *n* – low *k* absorber candidate is

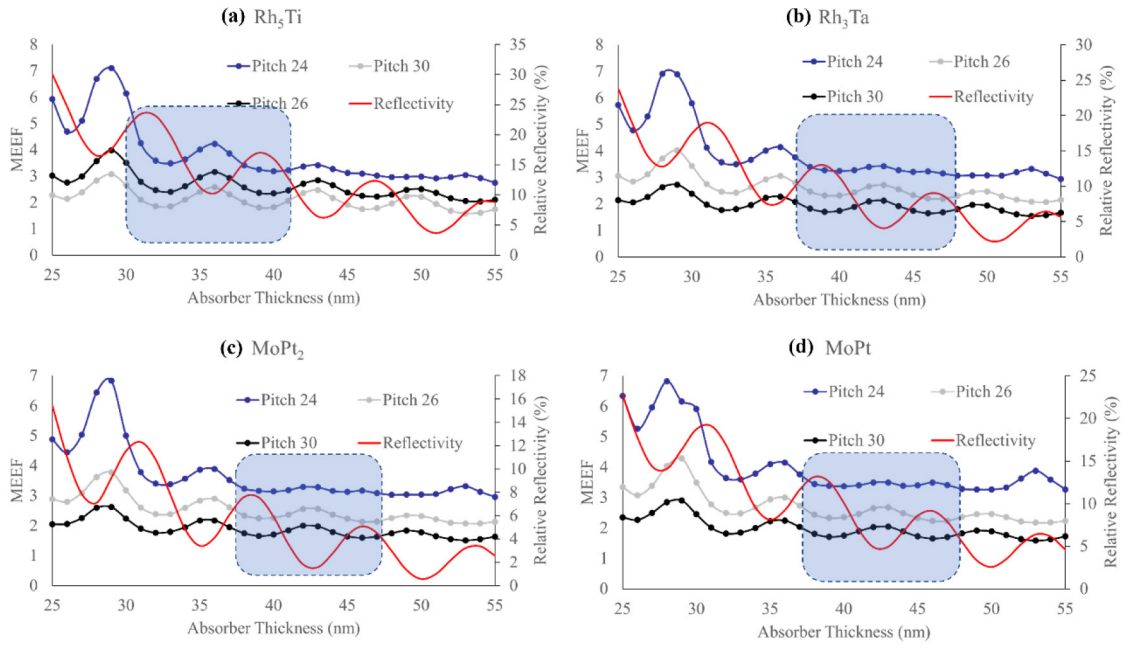

Figure 10. MEEF, reflectivity vs absorber thickness of 24nm, 26nm, and 30nm line/space pitch imaged using (a) Rh_5Ti mask absorber stack, (b) Rh_3Ta mask absorber stack, (c) $MoPt_2$ mask absorber stack and (d) MoPt mask absorber stack.

Table 2. Aerial image NILS for 36nm and 40nm pitch contact-holes array imaged using 42nm thick candidate absorbers along with associated reflectivity and phase shift values.

Absorber	NILS		Reflectivity (%)	Phase Shift (°)
	36nm	40nm		
Rh_5Ti @ 42m	2.50	2.58	9%	244.6°
Rh_3Ta @ 42m	2.50	2.58	5.2%	229.3°
$MoPt_2$ @ 42m	2.40	2.48	1.8%	219.6°
MoPt @ 42m	2.44	2.58	5%	206.5°

desired for a thin, high phase – high reflectivty PSM.

Contact-holes behave differently than the line/space pattern in terms of MEEF. The MEEF trend gradually decreases with increase in attPSM absorber reflectance. Furthermore, the MEEF trench does not coincide with reflectivity peak. Although higher NILS is obseverd for higher reflectivity, MEEF value dominates the mask absorber thickness. Care must be exercized in determinng the PSM reflectance to avoid priniting false contacts. Higher mask reflectance leads to smaller FCR ratio that may lead to a higher probability of stochastic failures. Co-optimization of NILS and MEEF indicate 42nm absorber thickness for contact-holes case. All 42nm attPSM absorber candidates have phase shift in the vicinty of 1.2π. Nearfield intensity response for 40nm pitch contact-hole with a 20nm opening show low intensity loss for all candidate alloys at higher illumniation angles compared to a 61nm Ta-based reference absorber. This indicates reduced effect of illumination conditions on imaging performance.

Similar co-optimization applied to additional test cases can help determine a robust optical design for PSM masks in EUV lithography. This can simplify and narrow the choice of material candidates.

6. References

[1] Armeanu, A., Philipsen, V., Jiang, F., Fenger, G. Lafferty, N., Gillijns, W., Hendrickx, E., and Sturtevant, J., "Enabling enhanced EUV lithographic performance using advanced SMO, OPC, and RET," **Proc. SPIE 10809**, 108090G, (2019).

[2] Sejpal, R., Philipsen, V., Armeanu, A., Wei, C.-I., Gillijns, W., Lafferty, N., Fenger, G., and Hendrickx, E., "Exploring alternative EUV mask absorber for iN5 self-aligned block and contact layers," **Proc. SPIE 11148**, 111481B (2019).

[3] Bisschop, P. D., "Stochastic effects in EUV lithography: random, local CD variability, and printing failures," *J. Micro- Nanolith. Mem.* 16(4), 041013 (2017).

[4] Tencor, K. L. A., "PROLITH," Version X5 1 (2015).

[5] Wiener, O., "Die Theorie des Mischkorpers fur das Feld der stationaren Stromung," Abhandlungen der Sachsischen Gesellschaft der Akademischen Wissenschaften, *J. Math. Phys. 32*, 507–604 (1912).

[6] Aspnes, D. E., "Optical properties of thin films," *Thin Solid Films 89*(3), 249–262 (1982).

[7] Bourov, A., "Optical properties of materials for 157 nm lithography," Theses, RIT (2003).

[8] ASM International, ed., [ASM handbook, 10th editon], ASM International, Materials Park, Ohio (1990).

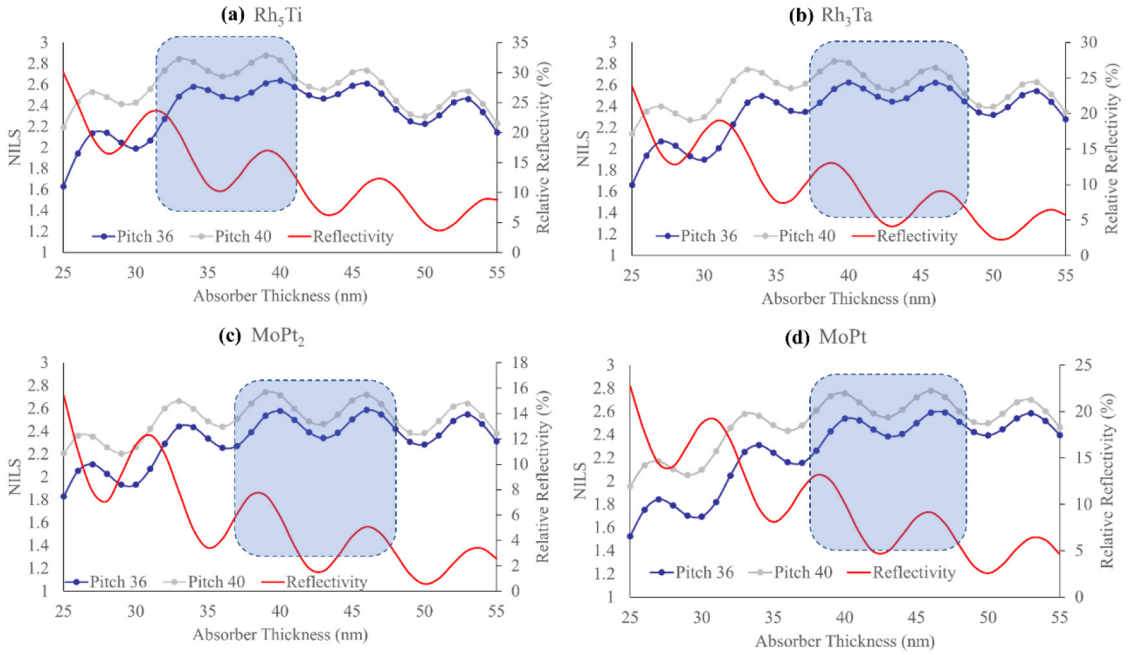

Figure 11. NILS, reflectivity vs absorber thickness of 36nm and 40nm pitch contact-holes arrays imaged using (a) Rh_5Ti mask absorber stack, (b) Rh_3Ta mask absorber stack, (c) $MoPt_2$ mask absorber stack and (d) MoPt mask absorber stack.

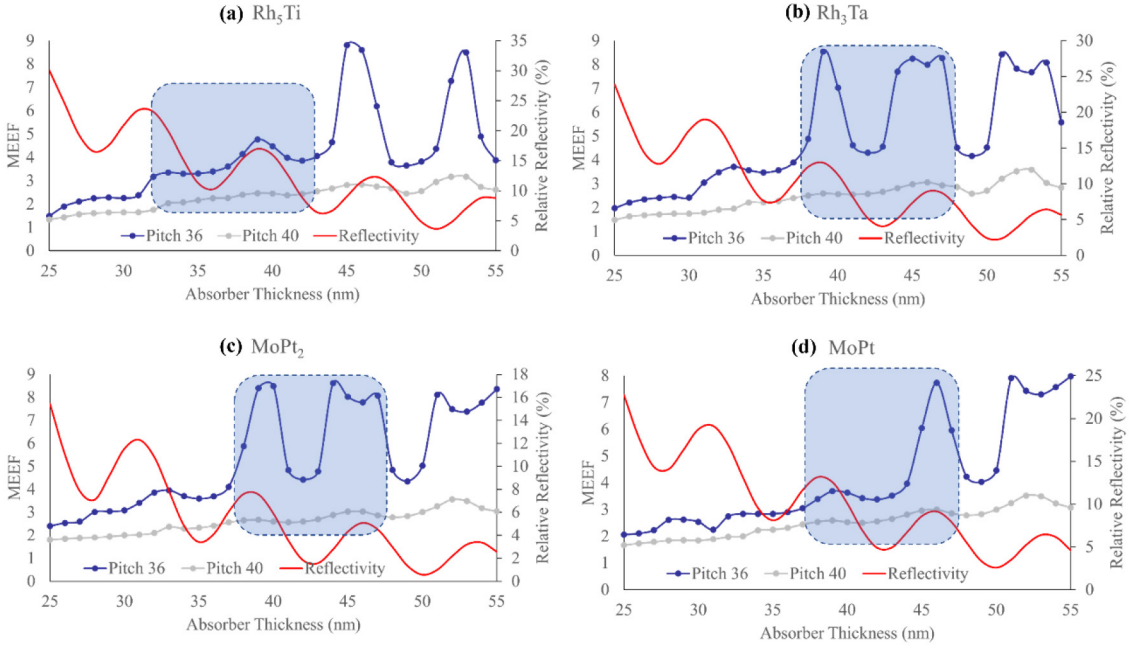

Figure 12. MEEF, reflectivity vs absorber thickness of 36nm and 40nm pitch contact-holes arrays imaged using (a) Rh_5Ti mask absorber stack, (b) Rh_3Ta mask absorber stack, (c) $MoPt_2$ mask absorber stack and (d) MoPt mask absorber stack.

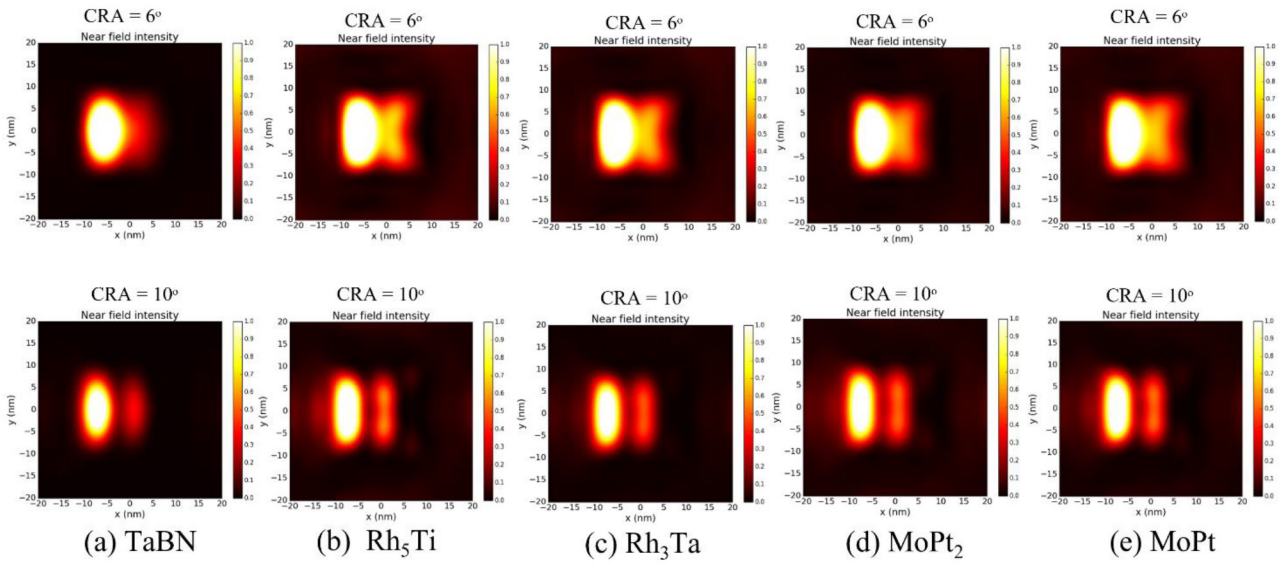

Figure 13. Reflected nearfield intensity at CRA = 6 and 10 for a 40nm pitch contact-holes pattern with a 20nm opening using (a) 61nm Ta-based reference absorber, (b) Rh_5Ti mask absorber stack, (c) Rh_3Ta mask absorber stack, (d) $MoPt_2$ mask absorber stack and (e) MoPt mask absorber stack. The reflected nearfield intensities are modelled using DrLitho simulator.[12]

[9] Lare, M.C. van, Timmermans, F. J., and Finders, J., "Alternative reticles for low-k1 EUV imaging," **Proc. SPIE 11147**, 111470D (2019).

[10] Lare, C. van, Timmermans, F., and Finders, J., "Mask-absorber optimization: the next phase," *J. Micro-Nanolith. Mem.* *19*(2), 024401 (2020).

[11] Erdmann, A., Evanschitzky, P., Mesilhy, H., Philipsen, V., Hendrickx, E., and Bauer, M., "Attenuated phase shift mask for extreme ultraviolet: can they mitigate three-dimensional mask effects?," *J. Micro-Nanolith. Mem.* *18*(1), 011005 (2018).

[12] "Computational Lithography and Optics.", Fraunhofer Institute for Integrated Systems and Device Technology IISB, https://www.iisb.fraunhofer.de/en/research_areas/simulation/lithography.html (8 July 2021).

BACUS N • E • W • S

Sponsorship Opportunities

Sign up now for the best sponsorship opportunities

Photomask Technology + EUV Lithography 2022
Contact: Melissa Valum
Tel: +1 360 685 5596; **melissav@spie.org**

Advanced Lithography + Patterning 2022
Contact: Teresa Roles-Meier
Tel: +1 360 685 5445; **teresar@spie.org**

Advertise in the BACUS News!

The BACUS Newsletter is the premier publication serving the photomask industry. For information on how to advertise, contact:

Melissa Valum
Tel: +1 360 685 5596
melissav@spie.org

BACUS Corporate Members

Acuphase Inc.
American Coating Technologies LLC
AMETEK Precitech, Inc.
Berliner Glas KGaA Herbert Kubatz GmbH & Co.
FUJIFILM Electronic Materials U.S.A., Inc.
Gudeng Precision Industrial Co., Ltd.
Halocarbon Products
HamaTech APE GmbH & Co. KG
Hitachi High Technologies America, Inc.
JEOL USA Inc.
Mentor Graphics Corp.
Molecular Imprints, Inc.
Panavision Federal Systems, LLC
Profilocolore Srl
Raytheon ELCAN Optical Technologies
XYALIS

Industry Briefs

Smart Cars to Drive LIDAR Market Growth

The market research firm Yole Development forecasts automotive and industrial applications will take the worldwide LIDAR (Light-Detection-and-Ranging) market from US$1.8 billion in 2020 to US$5.7 billion by 2026, a compound annual growth rate of 21%.

https://www.optica-opn.org/home/industry/2021/october/report_smart_cars_to_drive_lidar_market_growth/

IBM, Samsung Unveil VTFET to Extend Moore's Law

IBM and Samsung Electronics claimed a breakthrough in semiconductor design based on a new IBM architecture touted as enabling an 85% reduction in power consumption. The partners said the Vertical Transport Field-Effect Transistors (VTFET) scheme offers greater power efficiency over FinFET designs, potentially extending Moore's Law scaling beyond current two-dimensional nanosheet thresholds.

EETimes - IBM, Samsung Unveil VTFET to Extend Moore's Law

DoD Ramps Secure Chip Design Effort

Microsoft and Qualcomm Technologies will lead the second phase of a Pentagon chip initiative designed to leverage U.S. microelectronics capabilities while securing its technology supply chain. Both companies oversaw initial development beginning last year under the Defense Department's Rapid Assured Microelectronics Prototypes (RAMP) initiative. IBM was a phase-one partner with Microsoft.

https://www.eetimes.com/dod-ramps-secure-chip-design-effort/

Global Total Semiconductor Equipment Sales on Track to Top $100 Billion in 2021 for First Time, SEMI Reports.

Global sales of total semiconductor manufacturing equipment by original equipment manufacturers are forecast to reach a new high of $103 billion in 2021, surging 44.7% from previous industry record of $71 billion in 2020, SEMI announced today in releasing its Year-End Total Semiconductor Equipment Forecast - OEM Perspective at SEMICON Japan 2021. The growth is expected to continue with the global total semiconductor manufacturing equipment market expanding to $114 billion by 2022.

https://www.semiconductor-digest.com/global-total-semiconductor-equipment-sales-on-track-to-top-100-billion-in-2021-for-first-time-semi-reports/

Join the premier professional organization for mask makers and mask users!

About the BACUS Group

Founded in 1980 by a group of chrome blank users wanting a single voice to interact with suppliers, BACUS has grown to become the largest and most widely known forum for the exchange of technical information of interest to photomask and reticle makers. BACUS joined SPIE in January of 1991 to expand the exchange of information with mask makers around the world.

The group sponsors an informative monthly meeting and newsletter, BACUS News. The BACUS annual Photomask Technology Symposium covers photomask technology, photomask processes, lithography, materials and resists, phase shift masks, inspection and repair, metrology, and quality and manufacturing management.

Individual Membership Benefits include:

- Subscription to BACUS News (monthly)
- Eligibility to hold office on BACUS Steering Committee

spie.org/bacushome

Corporate Membership Benefits include:

- 3-10 Voting Members in the SPIE General Membership, depending on tier level
- Subscription to BACUS News (monthly)
- One online SPIE Journal Subscription
- Listed as a Corporate Member in the BACUS Monthly Newsletter

spie.org/bacushome

CALENDAR

2022

SPIE Advanced Lithography + Patterning
27 February - 3 March 2022
San Jose Convention Center
San Jose, California, USA
www.spie.org/al

Photomask Japan
26-28 April 2022
Digital Forum
www.photomask-japan.org

EMLC 2022
20-23 June
Leuven, Belgium
https://www.emlc-conference.com/

SPIE Photomask Technology + Extreme Ultraviolet Lithography
25-29 September 2022
Monterey, California, USA
www.spie.org/puv

SPIE, the international society for optics and photonics, brings engineers, scientists, students, and business professionals together to advance light-based science and technology. The Society, founded in 1955, connects and engages with our global constituency through industry-leading conferences and exhibitions; publications of conference proceedings, books, and journals in the SPIE Digital Library; and career-building opportunities. Over the past five years, SPIE has contributed more than $22 million to the international optics community through our advocacy and support, including scholarships, educational resources, travel grants, endowed gifts, and public-policy development. www.spie.org.

SPIE.
International Headquarters
P.O. Box 10, Bellingham, WA 98227-0010 USA
Tel: +1 360 676 3290
Fax: +1 360 647 1445
help@spie.org • spie.org

Shipping Address
1000 20th St., Bellingham, WA 98225-6705 USA

SPIE.EUROPE
2 Alexandra Gate, Ffordd Pengam, Cardiff,
CF24 2SA, UK
Tel: +44 29 2089 4747
Fax: +44 29 2089 4750
info@spieeurope.org • spieeurope.org

You are invited to submit events of interest for this calendar. Please send to lindad@spie.org.